

This document is confidential and is proprietary to the American Chemical Society and its authors. Do not copy or disclose without written permission. If you have received this item in error, notify the sender and delete all copies.

## Targeted polymeric nanoparticles for drug delivery to hypoxic, triple-negative breast tumors

|                               |  |
|-------------------------------|--|
| Journal:                      | <i>ACS Applied Bio Materials</i>   |
| Manuscript ID                 | mt-2020-013364.R3  |
| Manuscript Type:              | Article  |
| Date Submitted by the Author: | 07-Dec-2020  |
| Complete List of Authors:     | Mamnoon, Babak; North Dakota State University, Department of Pharmaceutical Sciences<br>Loganathan, Jagadish; North Dakota State University, Department of Pharmaceutical Sciences<br>Confeld, Matthew; North Dakota State University, Department of Pharmaceutical Sciences<br>Fonseka, Nimesha; North Dakota State University, Department of Pharmaceutical Sciences<br>Feng, Li; North Dakota State University, Department of Pharmaceutical Sciences<br>Froberg, Jamie; North Dakota State University, Department of Physics<br>Choi, Yongki; North Dakota State University, Physics<br>Tuvin, Daniel; Sanford Health Broadway Clinic<br>Sathish, Venkatachalem; North Dakota State University, Pharmaceutical Sciences<br>Mallik, Sanku; North Dakota State University, Department of Pharmaceutical Sciences |
|                               |  |

SCHOLARONE™  
Manuscripts

# Targeted polymeric nanoparticles for drug delivery to hypoxic, triple-negative breast tumors

Babak Mamnoon<sup>1</sup>, Jagadish Loganathan<sup>1</sup>, Matthew I. Confeld<sup>1</sup>, Nimesha De Fonseka<sup>1</sup>, Li Feng<sup>1</sup>, Jamie Froberg<sup>2</sup>, Yongki Choi<sup>2</sup>, Daniel M. Tuvin<sup>3</sup>, Venkatachalem Sathish<sup>1</sup>, Sanku Mallik<sup>1\*</sup>

<sup>1</sup>Department of Pharmaceutical Sciences, and <sup>2</sup>Department of Physics, North Dakota State University, Fargo, North Dakota 58102, United States. <sup>3</sup>Sanford Broadway Clinic, Fargo, North Dakota 58102, United States.

**\*Corresponding Author.** Sanku Mallik, Phone: 701-231-7888, Fax: 701-231-7831.

Email: [sanku.mallik@ndsu.edu](mailto:sanku.mallik@ndsu.edu)

## Abstract

High recurrence and metastasis to vital organs are the major characteristics of triple-negative breast cancer (TNBC). Low vascular oxygen tension promotes resistance to chemo- and radiation therapy. Neuropilin-1 (NRP-1) receptor is highly expressed on TNBC cells. The tumor-penetrating iRGD peptide interacts with the NRP-1 receptor, triggers endocytosis and transcytosis, and facilitates penetration. Herein, we synthesized a hypoxia-responsive diblock PLA–diazobenzene–PEG copolymer and prepared self-assembled hypoxia-responsive polymersomes (Ps) in an aqueous buffer. The iRGD peptide was incorporated into the polymersome structure to make hypoxia-responsive iRGD-conjugated polymersomes (iPs). Doxorubicin (DOX) was encapsulated in the polymersomes to prepare both targeted and non-targeted hypoxia-responsive polymersomes (DOX-iPs and DOX-Ps, respectively). The polymeric nanoparticles released less than 30% of their encapsulated DOX within 12 hours under normoxic conditions (21% oxygen), whereas under hypoxia (2% Oxygen), doxorubicin release remarkably increased to over 95%. The targeted polymersomes significantly decreased TNBC cells' viability in monolayer and spheroid cultures under hypoxia compared to normoxia. Animal studies displayed that targeted polymersomes significantly diminished tumor growth in xenograft nude mice. Overall, the targeted polymersomes exhibited potent anti-tumor activity in monolayer, spheroid, and animal models of TNBC. With further developments, the targeted nanocarriers discussed here might have the translational potential as drug carriers for the treatment of TNBC.

**Keywords:** Hypoxia, Nanotechnology, Polymersomes, Targeted Drug Delivery, Nanoparticles

## 1 2 3 1. Introduction 4 5

6 Breast cancer is a challenging disorder for women, regardless of the treatment strategy used.<sup>1</sup> A  
7 high recurrence rate and metastasis to different organs (e.g., lung, bone, liver, and lymph nodes)  
8 contribute to adverse outcomes.<sup>2</sup> Metastatic breast cancer claims about 40,000 lives in the US  
9 annually.<sup>3</sup> Triple-negative breast cancer (TNBC) is marked by the loss of all biomarker  
10 expression<sup>4</sup> and includes about 15% of all diagnosed breast malignancies.<sup>5</sup> Based on the gene  
11 expression profiles, there are four subtypes of TNBC.<sup>6</sup> Effective therapies are available for the  
12 estrogen, progesterone, and human epidermal growth factor receptor-positive subtypes.  
13 However, no promising treatment exists for TNBC other than systemic chemotherapy.<sup>7</sup> This is  
14 partially due to rapid cell proliferation and inadequate blood flow, which creates a low oxygen  
15 concentration (hypoxia) in tumors.<sup>8</sup> Notably, hypoxia is a primary driver of metastasis and  
16 aggressiveness in TNBC, which hinders treatment.<sup>9–11</sup>  
17  
18

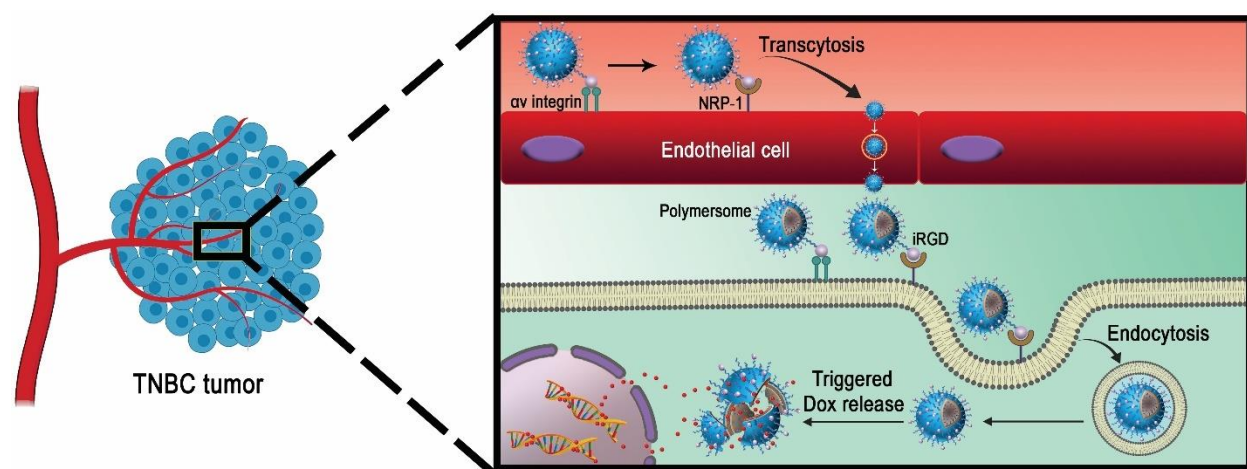
19 Due to the lack of specific targeting, chemotherapeutic drugs for TNBC inflict severe damage to  
20 healthy tissues. Besides, low solubility, decreased bioavailability, and accelerated clearance of  
21 drugs from the bloodstream make it challenging to achieve the desired clinical outcomes.<sup>12</sup> To  
22 address these problems, nanotechnology has emerged as a rapidly developing field to design  
23 drug carriers for TNBC treatment.<sup>13,14</sup> Drugs encapsulated in nanocarriers have several  
24 advantages compared to the free molecules. For instance, polymeric nanoparticles help increase  
25 lipophilic drugs' solubility by carrying these drugs within their bilayer.<sup>15–18</sup> Polyethylene glycol  
26 (PEG) on the outer layer extends the nanoparticles' circulation time and allows accumulation into  
27 the cancer tissues through enhanced permeability and retention (EPR) effect.<sup>19</sup> Nanoscale  
28 carriers with targeting moieties for the overexpressed surface receptors target the disease site,  
29 thus minimizing off-target side effects.<sup>20,21</sup> In addition, stimuli-responsive nanoparticles respond  
30 to specific triggers for releasing anticancer drugs only in the presence of a stimulus.<sup>22</sup>  
31  
32

33 Polymersomes are nanoparticles prepared from amphiphilic copolymers. Several properties  
34 render polymersomes more advantageous than other nanoparticles, including membrane  
35 stability, the tunable molecular weight of the polymers, ligand conjugation capacity, and more.<sup>23,24</sup>  
36 Hydrophobic molecules are encapsulated within the polymer bilayer, whereas hydrophilic drugs  
37 are incorporated into the aqueous core of the polymersomes, thereby carrying both types of drugs  
38 simultaneously.<sup>25</sup>  
39  
40

41 The tumor-penetrating iRGD peptide (CRGDKGPDC) contains the RGD motif for specific  
42 interactions with the overexpressed  $\alpha_v\beta_3$  integrins on endothelial cancer cells.<sup>26</sup> Subsequent  
43  
44

1  
2  
3 cleavage of iRGD peptide exposes the CendR (RGDK) motif with a higher binding affinity to the  
4 neuropilin-1 (NRP-1) receptor. This ligand-receptor binding promotes transcytosis and  
5 endocytosis, leading to tumor penetration.<sup>27</sup> Hence, surface conjugation of iRGD peptide to the  
6 drug-encapsulated polymersomes allows them to penetrate solid tumors<sup>28</sup> (Figure 1).  
7  
8

9  
10 Doxorubicin (DOX) is a common anthracycline drug used for treating various cancers, particularly  
11 TNBC.<sup>8,29</sup> DOX can be encapsulated into biocompatible nanocarriers to increase therapeutic  
12 index and sustained release.<sup>30</sup> In this study, we synthesized DOX-encapsulated, iRGD-  
13 conjugated, hypoxia-responsive, polymersomes (DOX-iPs) as targeted drug delivery vehicles to  
14 deliver DOX into solid tumors of TNBC. The targeted polymersomes offered here are dual-  
15 functional nanoparticles that bind specifically to the surface NRP-1 receptors and translate into  
16 TNBC cells. Then, the diazobenzene linker of the PLA-PEG polymer undergoes reduction within  
17 hypoxia, disintegrates the polymersome membrane, and releases encapsulated DOX in the tumor  
18 microenvironment. We also prepared non-targeted polymersomes (DOX-Ps) to evaluate their  
19 efficacy along with targeted polymersomes.  
20  
21



42  
43 **Figure 1.** Schematic illustration of the iRGD peptide-mediated targeting and penetration into the  
44 solid TNBC by the polymersomes.  
45  
46

## 47 **2. Materials and Methods**

### 48 **2.1. Chemicals**

49 The amino acids were purchased from Alfa Aesar. DPPE-lissamine rhodamine lipid dye was  
50 obtained from Avanti Polar Lipids. mPEG<sub>2000</sub>-NH<sub>2</sub> was bought from Biochempeg. All other  
51 chemicals for polymer synthesis were purchased from Millipore Sigma. The complete cell culture  
52  
53  
54

1  
2  
3 medium was obtained from VWR International. The antibiotic-antimycotic (Penicillin-  
4 Streptomycin-Amphotericin B) solution was purchased from Corning.  
5  
6  
7

## 8 **2.2. Synthesis and characterization of copolymers and targeting peptide**

  
9

10 The PLA<sub>8500</sub>-Azo-PEG<sub>2000</sub> polymer was synthesized in our laboratory, as previously reported.<sup>8</sup> The  
11 <sup>1</sup>H NMR, <sup>13</sup>C NMR, and gel permeation chromatography (GPC) were used to analyze the final  
12 product (Supporting Information, Figures S1-S3). As previously reported, a peptide synthesizer  
13 (Liberty Blue) was used for synthesizing Hex-iRGD in our laboratory.<sup>17</sup> The product (145 mg, 64%)  
14 was characterized by circular dichroism and mass spectrometry (Supporting Information, Figures  
15 S4-S5).  
16  
17

## 18 **2.3. Synthesis of PLA<sub>8500</sub>-PEG<sub>2000</sub>-iRGD polymer**

  
19

20 The PLA<sub>8500</sub>-PEG<sub>2000</sub>-N<sub>3</sub> polymer was synthesized in our laboratory, as previously reported.<sup>31</sup>  
21 [2+3]-cycloaddition reaction was carried out for conjugating Hex-iRGD to PLA<sub>8500</sub>-PEG<sub>2000</sub>-N<sub>3</sub>  
22 polymer, as previously reported.<sup>17</sup> The lyophilized product was freeze-dried (yield: 50%) and  
23 characterized by circular dichroism spectroscopy (Supporting Information, Figure S5).  
24  
25

## 26 **2.4. Preparation of the polymersomes encapsulating doxorubicin**

  
27

28 The fluorescent lipid DPPE-N-lissamine rhodamine (LR, 5%), PLA<sub>8500</sub>-Azo-PEG<sub>2000</sub> polymer  
29 (85%), and PLA<sub>8500</sub>-PEG<sub>2000</sub>-iRGD (10%) were used for preparing targeted doxorubicin-  
30 encapsulated polymersomes (DOX-iPs). LR (5%) and PLA<sub>8500</sub>-Azo-PEG<sub>2000</sub> polymer (95%) were  
31 used to make doxorubicin-encapsulated polymersomes (non-targeted polymersomes, DOX-Ps).  
32 Doxorubicin encapsulated polymersomes were prepared using the pH gradient method.<sup>29</sup> The  
33 method and chemicals used to prepare polymersomes were previously reported.<sup>8</sup>  
34  
35

## 36 **2.5. Preparation of plain polymersomes**

  
37

38 Plain (HEPES buffer-encapsulated) nanoparticles were made from the PLA<sub>8500</sub>-Azo-PEG<sub>2000</sub>  
39 polymer (95%) and LR dye (5%). Briefly, LR was air-dried to make a thin layer film. PLA<sub>8500</sub>-Azo-  
40 PEG<sub>2000</sub> polymer (100  $\mu$ L) was mixed with the dried LR and added dropwise into 1000  $\mu$ L 25 mM  
41 HEPES buffer (pH 7.4) and evaporated for 45 minutes. Subsequently, the mixture was sonicated  
42 for 1 hour and filtered by Sephadex G100 column. Plain polymersomes were the control for the  
43 cell cytotoxicity studies.  
44  
45  
46  
47  
48  
49  
50  
51  
52  
53  
54  
55  
56  
57  
58  
59  
60

**2.6. Characterization**

The charge and size of the polymersomes were measured by Dynamic Light Scattering (DLS) instrument (Malvern Zetasizer). All samples were measured five times, and the average was recorded.

Nanoparticle solutions (10  $\mu$ L, 1 mg/mL) were dried by nitrogen flow. A microscope (NT-MDT NTEGRA AFM) was employed for acquiring AFM images. Samples were prepared for transmission electron microscopic (TEM) images based on a reported protocol.<sup>8</sup>

**2.7. Release studies**

The release kinetics of the nanoparticles was carried out by preparing a mixture of targeted polymersomes, NADPH, and liver microsomes under hypoxic (2% oxygen) and normoxic (21% oxygen) conditions according to previously reported protocol from our laboratory.<sup>8</sup> The loading content and encapsulation efficiency of the drug in the vesicles were calculated by measuring absorbance at 480 nm.<sup>32</sup>

**2.8. Cell culture**

The MDA-MB-231 cells were purchased from American Type Culture Collection (Manassas, VA) and cultured as recommended by the vendor. For the normoxic conditions, cells were grown in an incubator at 37 °C containing 5% CO<sub>2</sub> and 21% oxygen. For the hypoxic conditions, cells were incubated in a hypoxia chamber (Biospherix C21) with 5% CO<sub>2</sub> and 2% oxygen at 37 °C.

**2.9. Neuropilin-1 protein expression**

The TNBC cells were seeded ( $2.5 \times 10^5$  cells/well) in cell culture plates and incubated in normoxic conditions. When the cells reached around 40 to 50% confluence, a set of plates were moved to the hypoxia chamber (2% oxygen). The cells were then incubated in both hypoxic and normoxic chambers, and their protein was collected after 24 hours. The whole-cell lysates were analyzed using 10% SDS polyacrylamide gel electrophoresis. Proteins were transferred on PVDF membranes before incubation with NRP-1 (Abcam) and  $\beta$ -Actin (Applied Biological Materials) primary antibodies. Protein bands were detected by imaging the membrane, and densitometry analysis was carried out by Image Studio v.5.2 software.

**2.10. Cellular uptake studies**

The cells were seeded (5,000 cells/well) in two 12-well tissue culture plates and incubated under 5% CO<sub>2</sub>. When the cells reached 80% confluence, they were washed with 1X PBS and

1  
2  
3 replenished with fresh cell culture media. Then, one of the plates was moved to the hypoxia  
4 chamber (2% oxygen) for one doubling time before starting the experiments. The cells in both  
5 plates were treated with iRGD-conjugated and non-conjugated polymersomes (targeted and non-  
6 targeted treatments, respectively, 20  $\mu$ L each) for three hours. The plates were then washed three  
7 times with PBS, and the cell nuclei were stained with DAPI (NucBlue, Invitrogen). The images  
8 were taken by a Leica fluorescence microscope and analyzed by the NIH ImageJ (version: 1.52a)  
9 software.  
10  
11

### 12 **2.11. Cell viability and cytotoxicity in monolayer cultures**

  
13

14 The cells were seeded (5,000 cells/well) in the plates and grown 24 hours. The wells containing  
15 the cells were categorized into five treatments: HEPES-buffer encapsulated polymersomes, non-  
16 targeted polymersomes (DOX-Ps), targeted polymersomes (DOX-iPs), free DOX, and control  
17 (only HEPES buffer). In these experiments, 1, 2, and 4  $\mu$ M of free DOX and the same amounts  
18 of drug-encapsulated polymersomes were used for 72 hours under hypoxic and normoxic  
19 conditions. For the cytotoxicity study, the cells were incubated with different concentrations of  
20 plain polymersomes (20 to 100  $\mu$ g/mL). The cytotoxicity was measured after 4 hours by recording  
21 the fluorescence (excitation at 560 nm and emission at 595 nm).  
22  
23

### 24 **2.12. Three-dimensional cytotoxicity studies**

  
25

26 The spheroids were prepared using a Nanoshuttle three-dimensional cell culture kit (Greiner Bio-  
27 one). The NanoShuttle nanoparticles (200  $\mu$ L) were added into 80-90% confluent MDA-MB-231  
28 cells for magnetizing the cells overnight. The cells were dislodged, counted, and 20,000 cells  
29 were transferred into each well. The plates were laid on top of magnetic spheroid drives for 15  
30 minutes to form spheroids and incubated for 24 hours. The wells were then categorized into five  
31 treatments and incubated for 72 hours in hypoxia and normoxia with three different doxorubicin  
32 concentrations (1, 2, and 4  $\mu$ M). The spheroids were then washed with PBS, transferred to new  
33 plates for growing 24 hours. Subsequently, the cytotoxicity was determined (same as monolayer  
34 cell viability assay).  
35  
36

### 37 **2.13. *In vivo* toxicity and anti-tumor efficacy**

  
38

39 The anti-tumor efficacy of the polymersomes was evaluated on tumor-bearing mouse models,  
40 following an approved IACUC protocol. The MDA-MB-231 cell suspension ( $10^6$  cells per mouse)  
41 was mixed in Matrigel (Corning) at a 1:1 ratio (total 200  $\mu$ L) and subcutaneously injected into the  
42 8-week-old female athymic nude mice (Envigo). Three weeks after injection, 30 mice with a tumor  
43  
44

1  
2  
3  
4  
5  
6  
7  
8  
9  
10  
11  
12  
13  
14  
15  
16  
17  
18  
19  
20  
21  
22  
23  
24  
25  
26  
27  
28  
29  
30  
31  
32  
33  
34  
35  
36  
37  
38  
39  
40  
41  
42  
43  
44  
45  
46  
47  
48  
49  
50  
51  
52  
53  
54  
55  
56  
57  
58  
59  
60

1  
2  
3 volume ranging from 50-80 mm<sup>3</sup> were randomly divided into five treatment groups. The treatment  
4 groups were vehicle, free DOX, polymersomes, non-targeted, and targeted nanoparticles. The treatment  
5 control and polymersome-only groups received saline and polymersomes, respectively. The other  
6 3 groups received 5 mg DOX/kg dose. All treatments were given twice per week for four weeks.  
7 The body weights and tumor volumes were evaluated once every three days. Two weeks after  
8 the treatment ended, all mice were euthanized, the tumors were excised, and weighed. The vital  
9 organs were dissected and fixed in 10% formalin for histological evaluation.  
10  
11  
12  
13

#### 14 **2.14. *In vivo* biodistribution**

15

16  
17 Tumor-bearing female athymic nude mice were i.v. injected with iRGD-polymersomes containing  
18 lissamine rhodamine fluorescent dye. The mice were then euthanized after 3 and 8 hours; the  
19 organs (lung, liver, and kidney) were excised and imaged. The fluorescence integral density of  
20 accumulated polymersomes in each organ tissue was analyzed.  
21  
22

#### 23 **2. 15. Statistical analysis**

24

25  
26 The statistical analyses were all processed using Origin software (Origin 9.3, Northampton,  
27 Massachusetts) and presented as mean  $\pm$  SEM. The significant statistical difference between  
28 normoxic and hypoxic conditions within treatment groups was evaluated by ANOVA.  
29  
30

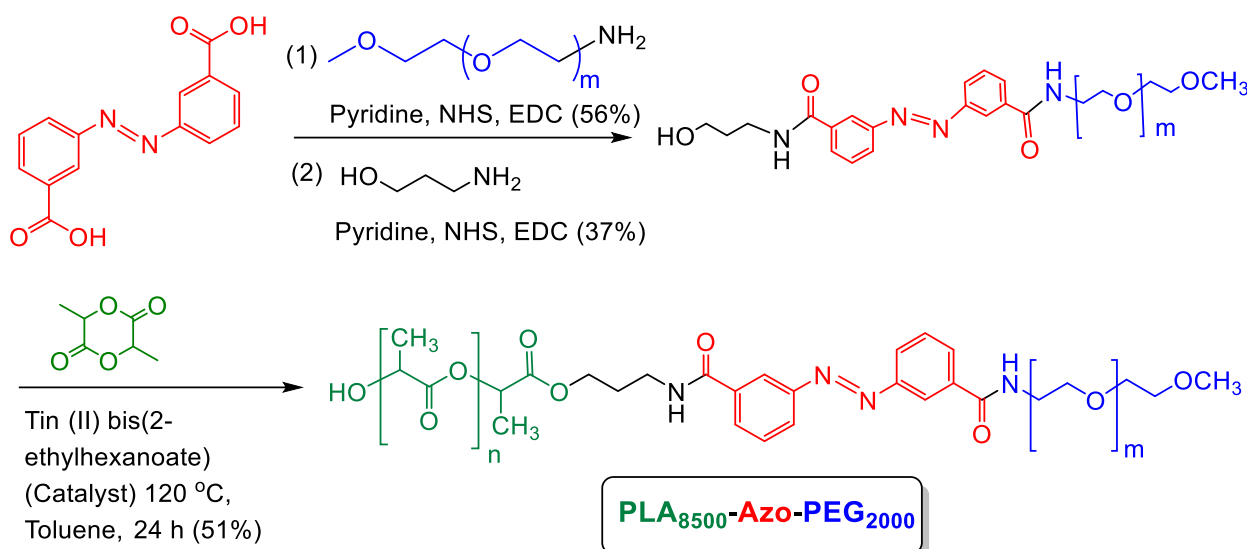
### 31 **3. Results and Discussion**

32  
33

#### 34 **3.1. Synthesis and characterization of polymersomes**

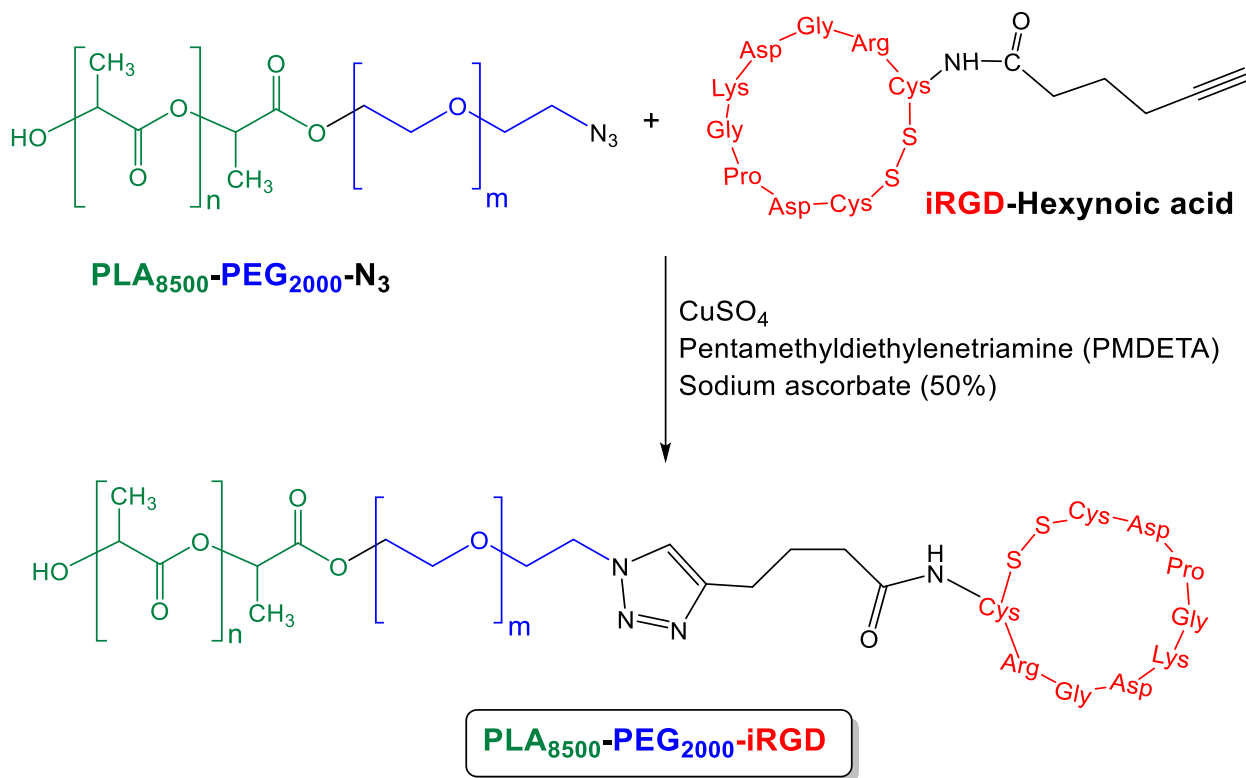
35

36  
37 Hypoxia contributes to the overall progression, migration, and invasion of TNBC and other solid  
38 tumors.<sup>33</sup> We synthesized PLA<sub>8500</sub>-Azo-PEG<sub>2000</sub> polymer with a hypoxia-responsive diazobenzene  
39 linker (Scheme 1 and Supporting Information, Figures S1, and S2), which self-assembles into  
40 polymersomes under appropriate conditions.  
41  
42  
43  
44



**Scheme 1.** Synthesis of the polymer with hypoxia-sensitive diazobenzene linker (green: PLA; red: hypoxia-responsive linker; blue: PEG).

The polydispersity index was calculated from Gel Permeation Chromatography to be 1.17 (Supporting Information, Figure S3). The surface PEG groups increase circulation time and the amount of polymersomes in cancerous tissue microenvironment by EPR effect.<sup>16</sup> The alkyne functional group on hexynoic acid was used for the conjugation of iRGD peptide to the azide (N<sub>3</sub>) functional group of PLA<sub>8500</sub>-PEG<sub>2000</sub>-N<sub>3</sub> polymer (Scheme 2). This peptide conjugation with the polymer was evaluated by circular dichroism spectroscopy (Supporting Information, Figure S5). We actively encapsulated doxorubicin into the nanoparticles, while unencapsulated doxorubicin was separated by passing the sample through a gel filtration column. A standard curve was plotted by measuring doxorubicin absorption as a function of concentration (Supporting Information, Figure S6). The encapsulation efficiency and loading of the non-targeted polymersomes were 51% and 9 weight percent, and for the targeted polymersomes were 63% and 11 weight percent, respectively. These polymersomes were stable over 8 weeks at 4 °C (Supporting Information, Figure S7).



**Scheme 2.** Reaction of PLA<sub>8500</sub>-PEG<sub>2000</sub>-N<sub>3</sub> polymer and Hex-iRGD.

The synthesized PLA<sub>8500</sub>-PEG<sub>2000</sub>-iRGD conjugate was then incorporated into the polymeric nanoparticles to prepare doxorubicin encapsulated hypoxia-responsive iRGD-conjugated polymersomes (DOX-iPs). The iRGD peptide on the polymersome first targets  $\alpha_v\beta_3$  and  $\alpha_v\beta_5$  integrins on the cells. Subsequent enzymatic cleavage exposes the CendR (RGDK) motif to interact with the NRP-1 receptors, cellular internalization, and endocytic transcytosis.<sup>34</sup> The size, charge, and polydispersity index (PDI) of the nanoparticles were measured by dynamic light scattering, DLS (Figure 2A, 2B, Table 1), and the spherical shape was confirmed by atomic force microscopic (AFM) imaging (Figure 2C, 2D). The nanoparticles' average size significantly changed in hypoxic conditions (Figure 2A S8, Table 1). Targeted vesicles indicated larger diameters because of the conjugation of the iRGD peptide. Figure 2B, S9, and Table 1). The slightly positive  $\zeta$  potential almost remained consistent within all conditions for non-targeted and targeted polymersomes (Table 1).

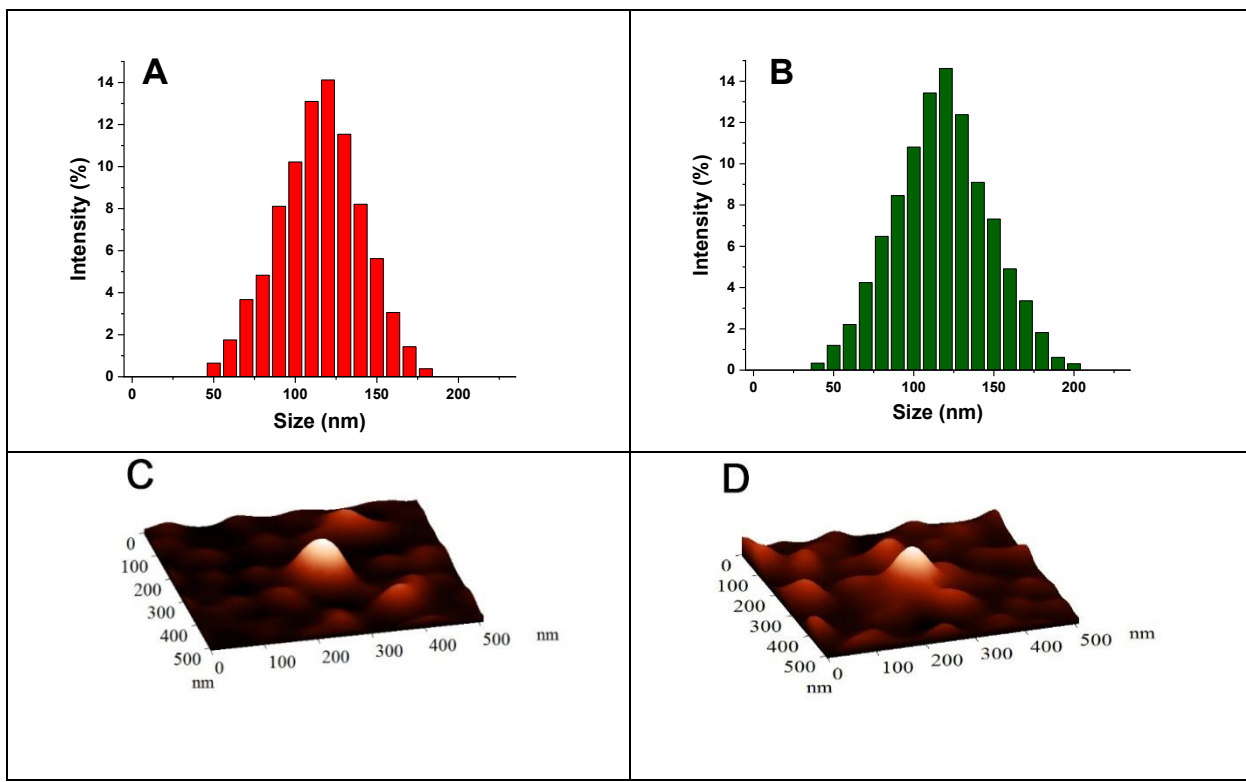


**Figure 2.** The size of non-targeted (**A**) and targeted (**B**) nanoparticles. AFM images of non-targeted (**C**) and targeted (**D**) nanoparticles.

**Table 1.** Diameter,  $\zeta$  potential, and PDI of different polymersomes.

| Polymersome         | Average diameter (nm) |                          | $\zeta$ potential (mV) |                 | PDI             |                 |
|---------------------|-----------------------|--------------------------|------------------------|-----------------|-----------------|-----------------|
|                     | Normoxia              | Hypoxia                  | Normoxia               | Hypoxia         | Normoxia        | Hypoxia         |
| <b>Non-targeted</b> | 118 $\pm$ 4           | 43 $\pm$ 4, 419 $\pm$ 22 | 0.13 $\pm$ 0.09        | 0.21 $\pm$ 0.11 | 0.13 $\pm$ 0.02 | 0.73 $\pm$ 0.16 |
| <b>Targeted</b>     | 136 $\pm$ 7           | 51 $\pm$ 3, 574 $\pm$ 27 | 0.23 $\pm$ 0.12        | 0.31 $\pm$ 0.14 | 0.18 $\pm$ 0.05 | 0.76 $\pm$ 0.19 |

### 3.2. Release studies in hypoxia and normoxia

Solid tumors have an environment that is rich in reducing agents.<sup>35</sup> The diazobenzene moieties in the polymers' structure undergo a four-electron reduction reaction in hypoxia, which leads to the disassembling of block polymers. This disintegrates the polymersomes and releasing the encapsulated drugs<sup>36</sup> (Figure 3A).

To check the drug release from polymersomes, targeted DOX-loaded polymersomes (DOX-iPs) were prepared. The release behavior was evaluated within hypoxic and normoxic conditions as a function of time (Figure 3B).

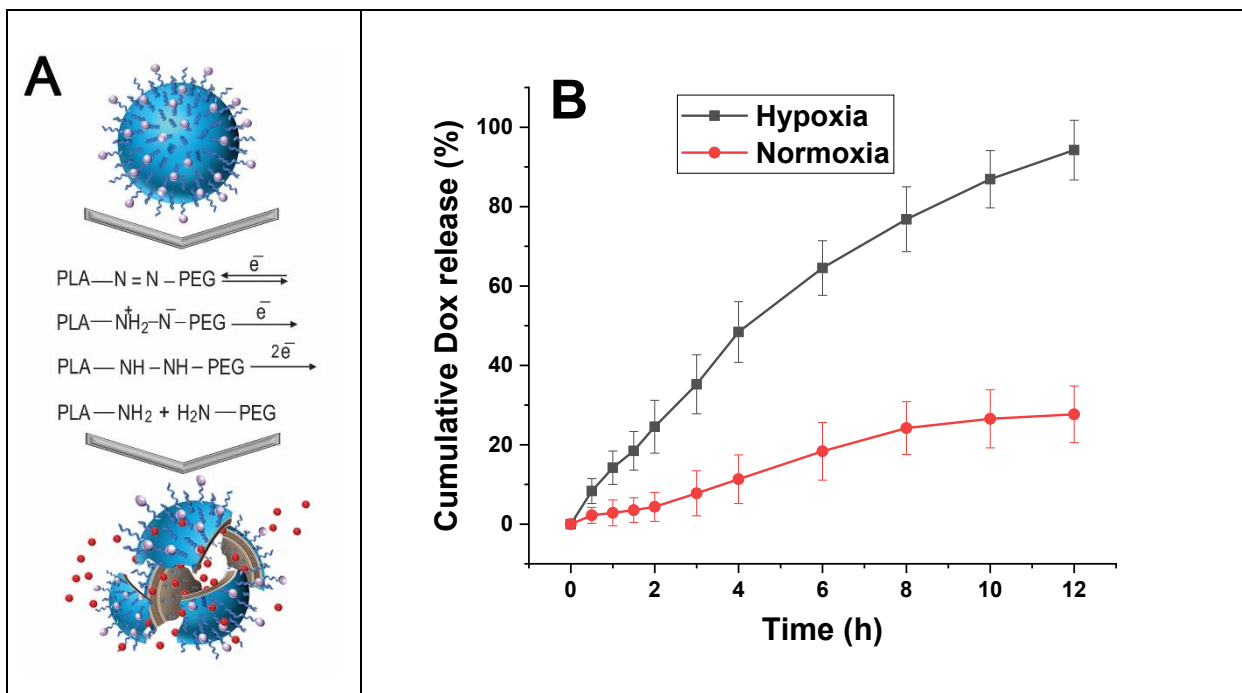


**Figure 3.** (A) Mechanism of the reduction under hypoxic environment. (B) DOX release in hypoxic (2% oxygen) and normoxic (21% oxygen) conditions ( $n = 3$ ).

The polymersomes released a significantly higher amount of Dox in hypoxia than normoxia. Polymersomes released about 95% of their encapsulated DOX in hypoxic conditions and about 25% in the normoxic condition in 12 hours. This confirmed that nanoparticles released their cargo due to the reduction of diazobenzene linker in hypoxia (Figure 3A).

AFM and TEM images showed that the nanoparticles' vesicular shape changed within hypoxia (Figure 4). Irregular morphology of the polymersomes in hypoxic conditions demonstrates possible disintegration and fusion of the polymeric vesicles (Figure 4B, 4D). We also observed that hypoxia decreased the hydrodynamic diameter and increased the vesicles' polydispersity index (Table 1).

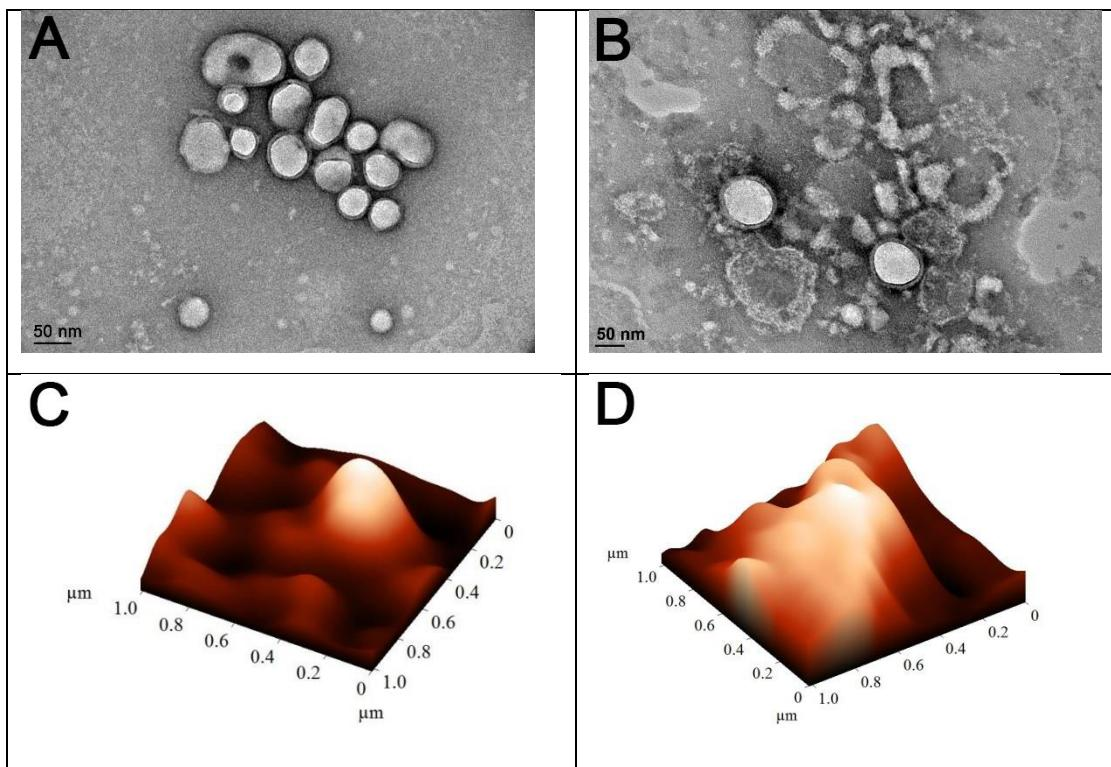


**Figure 4.** AFM and TEM images of the vesicles within normoxic (**A, C**) and hypoxic (**B, D**) conditions (scale bar: 50 nm).

### 3.3. Neuropilin-1 expression

To investigate any hypoxia-induced expression of NRP-1, the MDA-MB-231 cells grew under both normoxic (21% oxygen) and hypoxic (2% oxygen) conditions. Western blotting demonstrated a significant increase in NRP-1 protein expression within the cells cultured in hypoxia than normoxia (Figure 5). The protein  $\beta$ -actin used as an internal control. We found that the level of NRP-1 expression significantly increased after 24 hours within hypoxia (Figure 5B). This result suggested that hypoxia might structurally and functionally induce transmembrane NRP-1 protein expression through angiogenesis in TNBC cells.

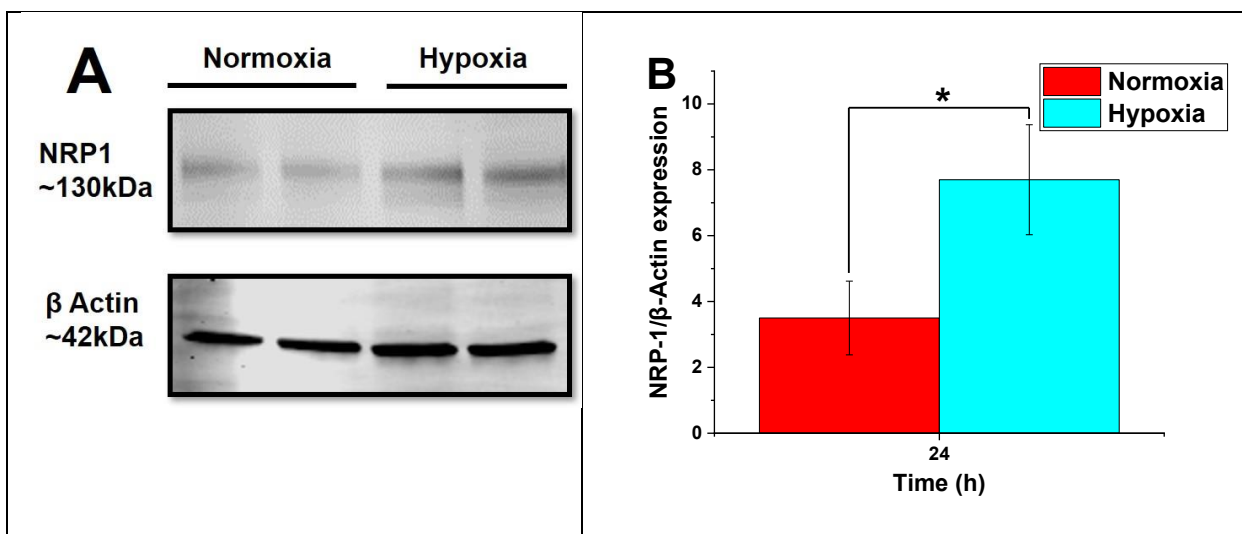


**Figure 5. (A)** NRP-1 expression in MDA-MB-231 cells with significant upregulation in hypoxic conditions (24h exposure). **(B)** The level of NRP-1/β-Actin expression ( $n = 3$ ,  $*p < 0.05$ ).

### 3.4. Cellular uptake

To demonstrate the nanoparticle penetration into TNBC cells, DPPE-lissamine rhodamine lipid (5%) was incorporated into the composition of polymersomes (without drug) to ease visualization fluorescence microscopic imaging.<sup>23,37</sup> The MDA-MB-231 cells were treated for 3 hours with both targeted and non-targeted polymersomes. The red fluorescence (lissamine rhodamine dye) was observed inside the cells treated with targeted nanoparticles under hypoxia. However, the cells incubated with non-targeted vesicles (control) did not show significant intensity of the red fluorescence inside the cells (Figure 6A) either in hypoxia or normoxia. The images' quantitative fluorescence integral density indicated a significant difference between the iRGD-targeted polymersomes in hypoxia and normoxia. The uptake results were significantly different for targeted and non-targeted polymersomes within hypoxia and normoxia (Figure 6B). It was found that the intensity of targeted nanoparticles was 8.5 times more than non-targeted polymersomes within the hypoxic condition and 3 times more than targeted nanoparticles within the normoxic condition. According to earlier studies, nanocarrier uptake in TNBC cells increases dynamically within the hypoxic condition.<sup>38</sup> Since TNBC cells overexpress the NRP-1 receptor on the surface,<sup>39</sup> targeted iRGD-conjugated polymersomes will show increased uptake within these cells. Besides, western blotting of MDA-MB-231 cells displayed an increased expression of NRP-1 under hypoxia. Based on these findings, we concluded that exposing the MDA-MB231 cells to iRGD-conjugated polymersomes for three hours elevated the cellular uptake.

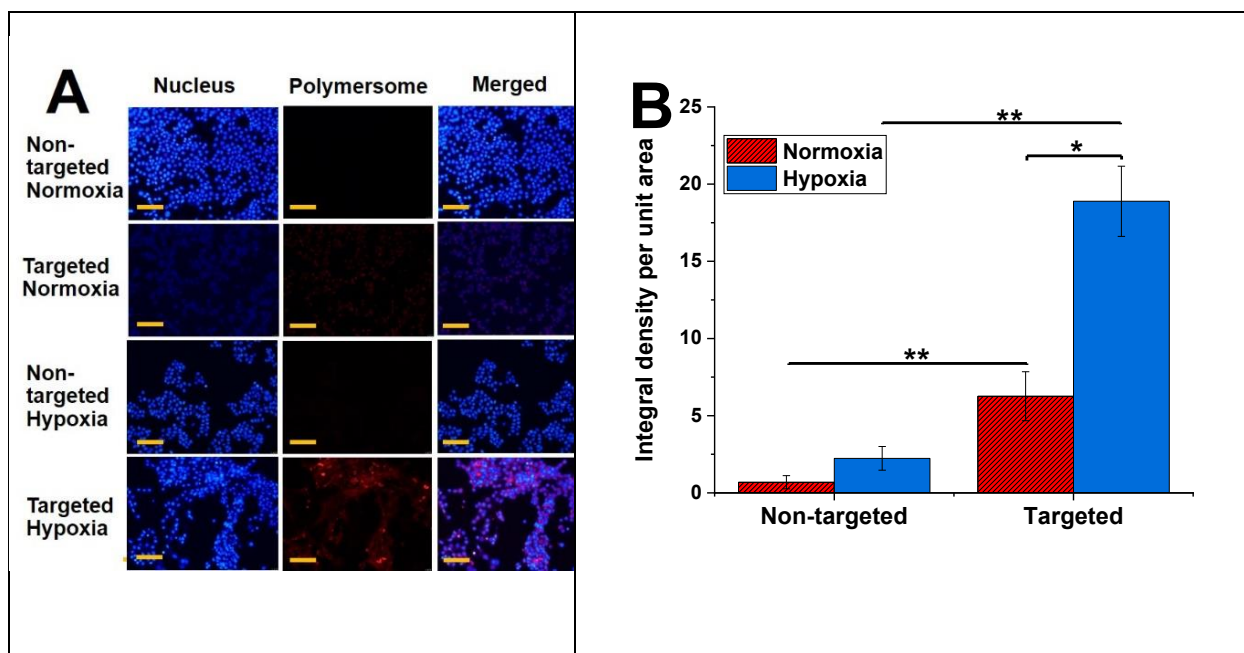


**Figure 6. (A)** Fluorescence microscopic images of polymersome uptake in MDA-MB-231 cells under hypoxia and normoxia (scale bar: 50  $\mu$ m). **(B)** Image intensity of polymersome uptake (n = 3, \*p < 0.05, \*\*p < 0.01).

### 3.5. Polymer toxicity and monolayer cytotoxicity

To assess polymer toxicity, the cells were treated with different amounts of the polymersomes encapsulating HEPES buffer within hypoxia and normoxia for 3 days. The polymersomes demonstrated more than 88% cell viability with a maximum of 100  $\mu$ g/mL polymer concentration (Figure 7A), indicating minimal toxicity. To demonstrate polymersomes' efficacy, the MDA-MB-231 monolayer cultures were treated for 3 days using four groups: control (no treatment, HEPES buffer only), free drug, non-targeted, and targeted nanoparticles. The results demonstrated that incubating the MDA-MB-231 cells with 4  $\mu$ M DOX encapsulated within targeted polymersomes under hypoxia reduced cell viability to 28% compared to normoxia (Figure 7B, p < 0.05). It was observed that targeted vesicles were more effective than non-targeted polymersomes and free DOX to kill TNBC cells under hypoxia. This is likely due to the binding of tumor-homing iRGD peptide on the targeted polymersomes with the overexpressed NRP-1 receptors on TNBC cells. According to drug release study (Figure 3B), nanoparticles released one-third (33%) of their loaded DOX within 3 h and around 79% within 8 h. Therefore, 3-day treatment will ensure enough

time for the polymersomes to translocate the breast cancer cells, break open, and release their drug cargo within the cells.

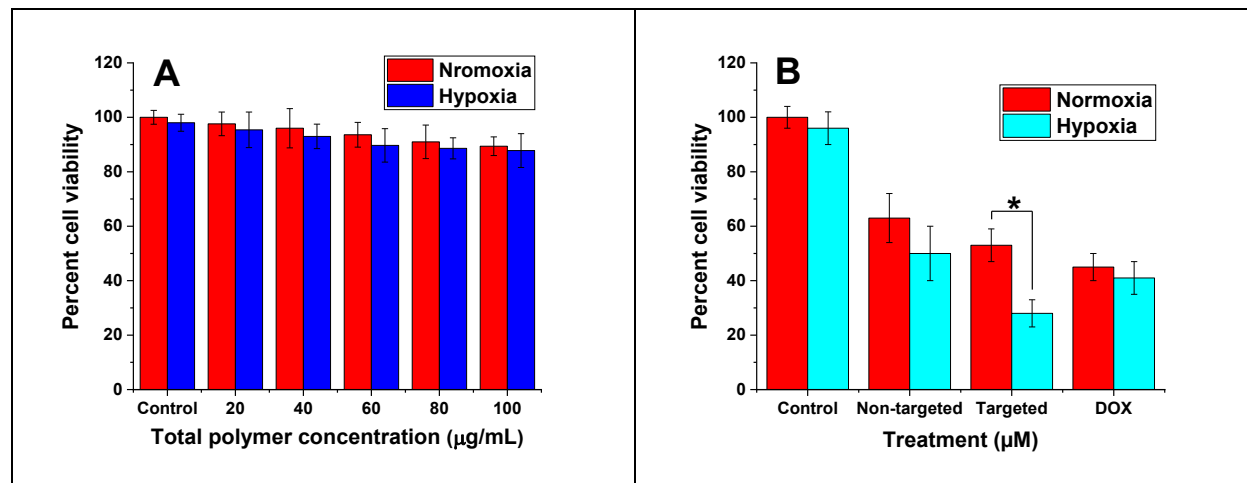


**Figure 7.** Viability of MDA-MB231 cells (monolayer) after 3-day treatment with buffer-encapsulated polymersomes (A,  $n = 6$ ), free DOX, non-targeted, and targeted polymersomes (B,  $n = 3$ , \*  $P < 0.05$ ).

### 3.6. Cell viability in spheroid cultures

The MDA-MB-231 three-dimensional spheroids were cultured for 3 days in hypoxic and normoxic conditions with the same treatment groups as a monolayer cell viability study (Figure 8A). The results indicated that under hypoxia, the cell viability was significantly diminished to 36% when the spheroids were incubated with 4 µM DOX loaded within targeted vesicles in contrast to non-targeted vesicles within the normoxic condition (66%) (Figure 8B). However, there was no significant difference in viability when the cells were incubated with non-targeted vesicles or free drug within hypoxic and normoxic conditions. This might reflect the slow diffusion of non-targeted nanoparticles and DOX inside the three-dimensional cultures. Instead, targeted polymersomes showed enhanced cytotoxicity based on receptor-mediated cell penetration. Some polymersomes might release the encapsulated DOX in the extracellular regions. In this regard, the free drug penetrates the cells via the cell membrane.<sup>40</sup> However, passive diffusion could be less prevalent in comparison with targeted drug-encapsulated nanoparticle delivery.

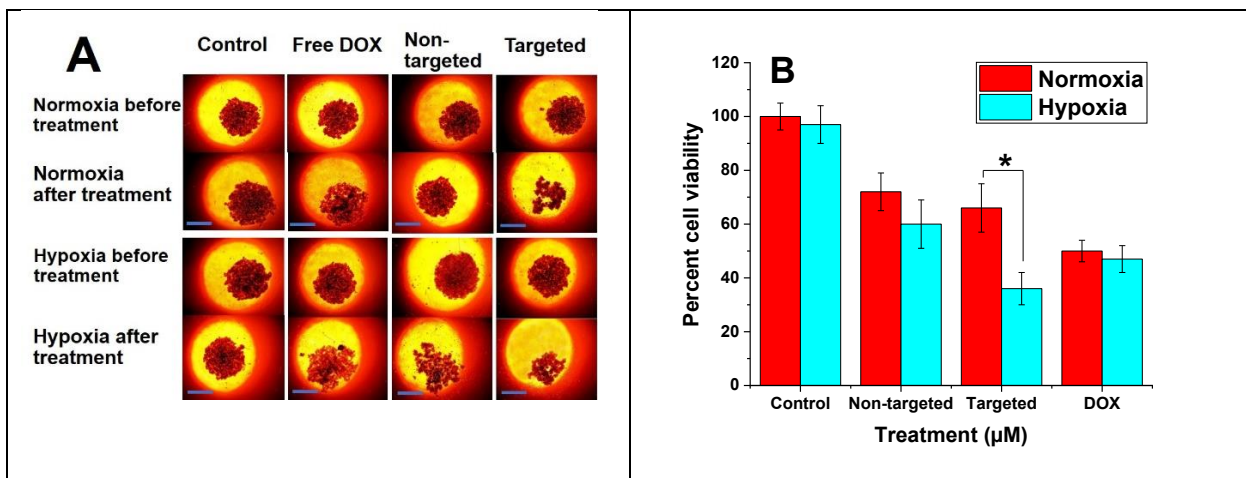


**Figure 8.** (A) Three-dimensional MDA-MB-231 spheroid images before and after incubating the cells with non-targeted and targeted vesicles under hypoxic and normoxic conditions (scale bar: 100  $\mu\text{m}$ ). (B) Viability of MDA-MB-231 cell spheroids ( $n = 3$ , \*  $P < 0.05$ ).

### 3.7. *In vivo* anti-tumor efficacy

To evaluate the anti-tumor efficacy, MDA-MB-231 tumor-bearing female nude mice were administered through the tail vein with saline (control), DOX, plain polymersomes, non-targeted, and targeted DOX-polymersomes twice per week for 4 weeks. Mice were monitored daily for the drugs' potential toxicity, and the tumor volume and body weight were calculated once every three days. The percent tumor volume growth within days was calculated (Figure 9A) and suggested tumor growth inhibition in all DOX-treated groups compared to the control. The tumor growth in the group treated with plain polymersomes demonstrated a slight difference compared to the saline group. Free DOX showed an increase of 337% in tumor volume. Non-targeted polymersomes exhibited a 253% increase in tumor volume that was significantly different compared to the saline group. However, targeted DOX-encapsulated nanoparticles demonstrated a much lower growth in the volume (129%) and displayed a significant difference in comparison with non-targeted vesicles, DOX, and saline ( $p < 0.05$  vs. non-targeted polymersomes  $p < 0.01$  vs. free DOX, and  $p < 0.001$  vs. saline). This suggested that targeted polymersomes were the most effective nanoparticles to inhibit TNBC tumor growth. After six weeks, we euthanized the animals, removed and weighed the tumors (Figure 9B).

The plain polymersomes, free DOX, and non-targeted polymersome treatment groups revealed the average tumor weights of 0.712, 0.661, and 0.565 g, respectively. However, the targeted polymersome treatment group resulted in the lowest average tumor weight of 0.312 g, significantly different compared to DOX treated groups and saline ( $p < 0.05$  vs. non-targeted,  $p < 0.01$  vs. free

DOX, and  $p < 0.001$  vs. saline). The percent tumor growth inhibition (TGI) was determined based on DOX treated groups' tumor volume compared to the saline tumor volume group (Figure 9C). The free DOX and non-targeted polymersome groups presented TGI of 41% and 55.7%, respectively. However, targeted polymersome treatment groups demonstrated a TGI of 77.6% that was significantly higher than non-targeted polymersome and free DOX treatment groups. Excised tumors in all treatment groups were dissected in half and imaged (Figure 9D). Overall, the expected high anti-tumor efficacy of the targeted polymersomes might be due to the defective tumor vasculature, enhanced blood circulation and accumulation within the tumors via surface-modified tumor penetrating iRGD peptide,<sup>36</sup> disintegration within hypoxic niches of breast tumors based on the presence of hypoxia-responsive moiety, and liberation of the drug within the cells.

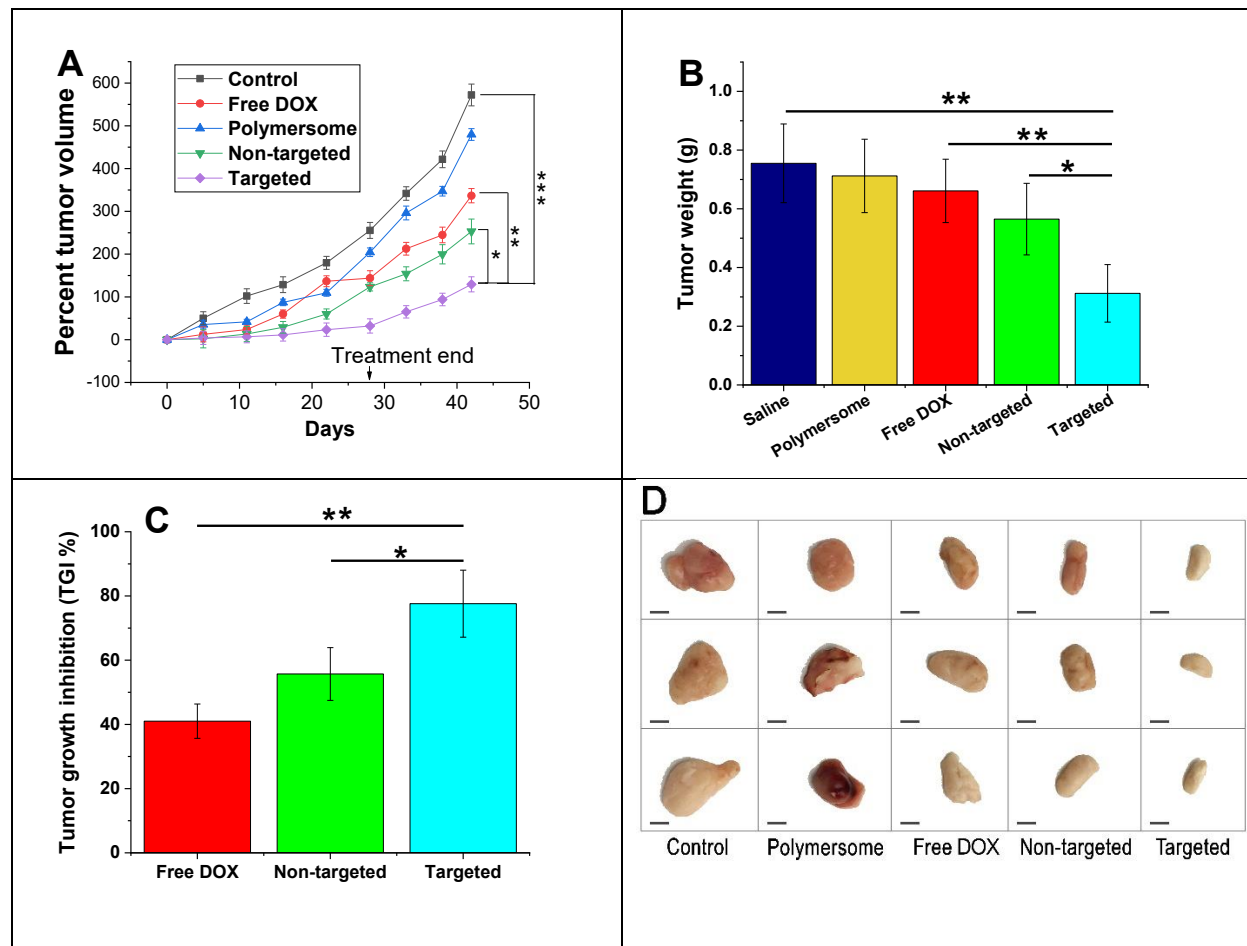


**Figure 9.** *In vivo* anti-tumor efficacy studies **(A)** Tumor volume growth of MDA-MB-231 cancer xenografts treated with saline, plain polymersomes, DOX, targeted, and non-targeted polymersomes with a dose of 5 mg DOX/kg. **(B)** Average tumor weight of all treatment groups ( $n = 3$ ,  $*p < 0.05$ ,  $**p < 0.01$ ). **(C)** Percent tumor growth inhibition (TGI) of DOX treated groups ( $n = 3$ ,  $*p < 0.05$ ,  $**p < 0.01$ ). **(D)** Excised tumor images from outside (scale bar: 5 mm).

### 3.8. *In vivo* toxicity of polymersomes

To determine the polymersomes' toxicity, main organs (lung, liver, and kidney) were collected at the end of the experiment and evaluated using histological assessments (hematoxylin and eosin staining, Figure 10). Histological analyses of mice treated with saline demonstrated some metastatic lesions within the liver tissue (black arrows) due to the diffusion of neoplastic cells through the vessels. The mice treated with DOX, non-targeted, and targeted nanoparticles did not show any metastatic lesion or toxicity. This presented substantial tumor growth inhibition and anti-tumor efficacy of the polymersome formulations and free drug. We did not evaluate heart tissue lesions in our study. However, possible toxicity might be expected with high doses of DOX to create myocardial damaged fibers. Overall, most of the organs treated with DOX-loaded vesicles were normal with no tissue necrosis or cell lesion. The histological evaluations demonstrated that non-targeted and targeted polymersomes delivered their drug cargo into the tumor tissues, enhanced anti-tumor efficacy, and reduced off-target toxicity.

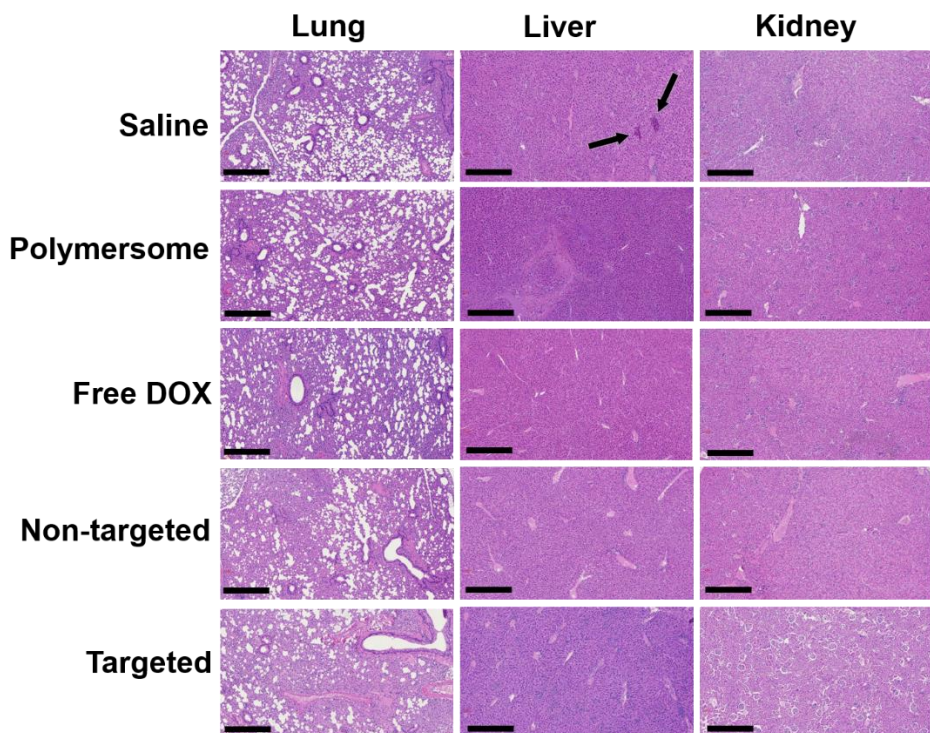


**Figure 10.** Histological assessment of lung, liver, and kidney tissues of nude mice after treating with control, free DOX, non-targeted, targeted, and plain polymersomes (scale bar: 100  $\mu$ m, 10x objective). In the saline-treated group, liver tissues demonstrated metastatic lesions (black arrows).

### 3.9. Biodistribution and nanoparticle accumulation

To assess the biodistribution of the targeted polymersomes, fluorescently labeled iRGD-conjugated polymersomes were injected via the tail vein into the female nude mice. The mice were euthanized at predetermined time points, and the liver, kidney, and lung were excised and imaged (Figure 11A). We did not observe any significant polymersome accumulation within organs after either 3 h or 8 h post-injection. The biodistribution study showed that targeted nanoparticles might selectively accumulate within the tumor tissues and reduce off-target organ cytotoxicity. The fluorescence integral density of nanoparticle accumulation within organ tissues was calculated by NIH ImageJ software (Figure 11B).

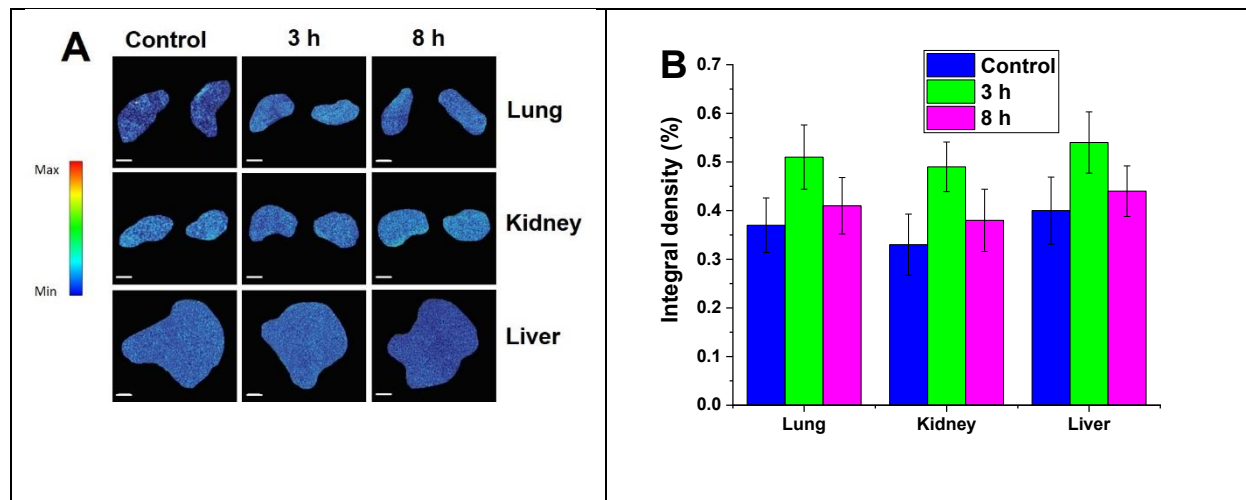


**Figure 11.** (A) Biodistribution to organs at 3 h and 8 h post-injection of indocyanine green-loaded iRGD-polymersomes ( $n = 3$ ) (scale bar: 2 mm). (B) Accumulation of targeted Polymersomes in organs after 3 h and 8 h post-injection of polymersomes ( $n = 3$ ).

### 4. Conclusion

We synthesized an amphiphilic diblock copolymer with a hypoxia-responsive diazobenzene linker capable of self-assembly into polymersomes. Doxorubicin was successfully encapsulated into the polymersomes. The tumor-targeting and penetrating iRGD peptide was conjugated into the polymersomes via click chemistry to make targeted hypoxia-responsive polymersomes. Targeted polymersomes exhibited higher cytotoxicity on TNBC cells in hypoxia than normoxia in monolayer and three-dimensional spheroid cell cultures. *In vivo* studies on TNBC tumor-bearing, nude mice demonstrated that targeted polymersomes had enhanced anti-tumor efficacy compared to non-targeted polymersomes and free doxorubicin. These drug-loaded polymer nanoparticles

1  
2  
3 demonstrated no toxicity against various internal organs, such as the liver, kidney, and lung. This  
4 is the first administration of hypoxia-responsive iRGD-polymersomes encapsulating doxorubicin  
5 in animal models of triple-negative breast cancer. An earlier study has demonstrated tumor  
6 suppression by employing doxorubicin within hypoxia-responsive nanoparticles to reach the  
7 TNBC tumors via the EPR effect.<sup>41</sup> The nanoparticles in our study are hypoxia-responsive and  
8 iRGD-conjugated. Hence, they offer the benefit of selective delivery of doxorubicin to TNBC  
9 tumors via active receptor-mediated targeting and enhanced penetration into the cells while  
10 lowering the off-target toxicity compared to passive tumor diffusion of nanoparticles or free drugs.  
11 The inclusion of diazobenzene hypoxia-responsive moiety contributes to the selective release of  
12 chemotherapeutics within breast tumors' hypoxic niches. The results of this study indicated that  
13 targeted hypoxia-responsive polymersomes could be administered for effective anticancer drug  
14 delivery into solid tumors of TNBC.  
15  
16  
17  
18  
19  
20  
21  
22  
23  
24

## 25 Acknowledgments

26

27 SM and VS acknowledge the support from NIH (NIGMS) grants 2R01GM 114080 and U54  
28 GM12872 and partial support from NSF EPSCoR Track-1 Cooperative Agreement OIA #1946202.  
29 Any opinions, findings, and conclusions or recommendations expressed in this material are those  
30 of the author(s) and do not necessarily reflect the views of the NSF. Ms. Parinaz Ghanbari  
31 prepared the illustrations. SM and VS acknowledge support from the NIGMS COBRE award  
32 1P20 GM109024 for the Animal Core Facility.  
33  
34  
35  
36

## 39 Appendix A. Supplementary data

40

41 The following is Supplementary data to this research:

42 <sup>1</sup>H NMR spectrum of the hypoxia-responsive polymer PLA<sub>8500</sub>–diazobenzene–PEG<sub>2000</sub>, <sup>13</sup>C NMR  
43 spectrum of the hypoxia-responsive polymer PLA<sub>8500</sub>–diazobenzene–PEG<sub>2000</sub>, GPC in THF of the  
44 hypoxia-responsive polymer PLA<sub>8500</sub>–diazobenzene–PEG<sub>2000</sub>, MALDI-TOF mass spectrum of the  
45 synthesized iRGD peptide, circular dichroism (CD) spectrum of the synthesized iRGD peptide, a  
46 calibration curve of doxorubicin hydrochloride solution, polymersome stability at 4 °C.  
47  
48  
49  
50  
51  
52  
53  
54  
55  
56  
57  
58  
59

1  
2  
3  
4  
5  
6  
7  
8  
9  
10  
11  
12  
13  
14  
15  
16  
17  
18  
19  
20  
21  
22  
23  
24  
25  
26  
27  
28  
29  
30  
31  
32  
33  
34  
35  
36  
37  
38  
39  
40  
41  
42  
43  
44  
45  
46  
47  
48  
49  
50  
51  
52  
53  
54  
55  
56  
57  
58  
59  
60

### References

(1) Yan, J.; Liu, Z.; Du, S.; Li, J.; Ma, L.; Li, L. Diagnosis and Treatment of Breast Cancer in the Precision Medicine Era. *Methods Mol Biol* **2020**, *2204*, 53–61. [https://doi.org/10.1007/978-1-0716-0904-0\\_5](https://doi.org/10.1007/978-1-0716-0904-0_5).

(2) Grobmyer, S. R.; Zhou, G.; Gutwein, L. G.; Iwakuma, N.; Sharma, P.; Hochwald, S. N. Nanoparticle Delivery for Metastatic Breast Cancer. *Nanomedicine: Nanotechnology, Biology and Medicine* **2012**, *8*, S21–S30. <https://doi.org/10.1016/j.nano.2012.05.011>.

(3) Gold, J.; Winer, E. P. Chemotherapy for Metastatic Breast Cancer. *The Breast: Comprehensive Management of Benign and Malignant Disease* **2009**, 1233–1261.

(4) Mehanna, J.; Haddad, F. G.; Eid, R.; Lambertini, M.; Kourie, H. R. Triple-Negative Breast Cancer: Current Perspective on the Evolving Therapeutic Landscape. *Int J Womens Health* **2019**, *11*, 431–437. <https://doi.org/10.2147/IJWH.S178349>.

(5) Dawson, S. J.; Provenzano, E.; Caldas, C. Triple Negative Breast Cancers: Clinical and Prognostic Implications. *European Journal of Cancer* **2009**, *45*, 27–40. [https://doi.org/10.1016/S0959-8049\(09\)70013-9](https://doi.org/10.1016/S0959-8049(09)70013-9).

(6) Lehmann, B. D.; Bauer, J. A.; Chen, X.; Sanders, M. E.; Chakravarthy, A. B.; Shyr, Y.; Pietenpol, J. A. Identification of Human Triple-Negative Breast Cancer Subtypes and Preclinical Models for Selection of Targeted Therapies. *J Clin Invest* **2011**, *121* (7), 2750–2767. <https://doi.org/10.1172/JCI45014>.

(7) Lebert, J. M.; Lester, R.; Powell, E.; Seal, M.; McCarthy, J. Advances in the Systemic Treatment of Triple-Negative Breast Cancer. *Curr Oncol* **2018**, *25* (Suppl 1), S142–S150. <https://doi.org/10.3747/co.25.3954>.

(8) Mamnoon, B.; Feng, L.; Froberg, J.; Choi, Y.; Sathish, V.; Mallik, S. Hypoxia-Responsive, Polymeric Nanocarriers for Targeted Drug Delivery to Estrogen Receptor-Positive Breast

1  
2  
3      Cancer Cell Spheroids. *Mol. Pharmaceutics* **2020**, *17* (11), 4312–4322.  
4  
5      <https://doi.org/10.1021/acs.molpharmaceut.0c00754>.  
6  
7 (9) Gilkes, D. M.; Semenza, G. L.; Wirtz, D. Hypoxia and the Extracellular Matrix: Drivers of  
8      Tumour Metastasis. *Nat Rev Cancer* **2014**, *14* (6), 430–439.  
9  
10     <https://doi.org/10.1038/nrc3726>.  
11  
12 (10) Hoffmann, C.; Mao, X.; Brown-Clay, J.; Moreau, F.; Absi, A. A.; Wurzer, H.; Sousa, B.;  
13     Schmitt, F.; Berchem, G.; Janji, B.; Thomas, C. Hypoxia Promotes Breast Cancer Cell  
14     Invasion through HIF-1 $\alpha$ -Mediated up-Regulation of the Invadopodial Actin Bundling  
15     Protein CSRP2. *Sci Rep* **2018**, *8* (1), 1–14. <https://doi.org/10.1038/s41598-018-28637-x>.  
16  
17 (11) Semenza, G. L. The Hypoxic Tumor Microenvironment: A Driving Force for Breast Cancer  
18     Progression. *Biochimica et Biophysica Acta (BBA) - Molecular Cell Research* **2016**, *1863*  
19     (3), 382–391. <https://doi.org/10.1016/j.bbamcr.2015.05.036>.  
20  
21 (12) Liu, J.; Guo, X.; Luo, Z.; Zhang, J.; Li, M.; Cai, K. Hierarchically Stimuli-Responsive  
22     Nanovectors for Improved Tumor Penetration and Programed Tumor Therapy. *Nanoscale*  
23     **2018**, *10* (28), 13737–13750. <https://doi.org/10.1039/C8NR02971G>.  
24  
25 (13) Cuenca, A. G.; Jiang, H.; Hochwald, S. N.; Delano, M.; Cance, W. G.; Grobmyer, S. R.  
26     Emerging Implications of Nanotechnology on Cancer Diagnostics and Therapeutics.  
27     *Cancer* **2006**, *107* (3), 459–466. <https://doi.org/10.1002/cncr.22035>.  
28  
29 (14) Shi, J.; Kantoff, P. W.; Wooster, R.; Farokhzad, O. C. Cancer Nanomedicine: Progress,  
30     Challenges and Opportunities. *Nature Reviews Cancer* **2017**, *17* (1), 20–37.  
31  
32     <https://doi.org/10.1038/nrc.2016.108>.  
33  
34 (15) Thambi, T.; Deepagan, V. G.; Yoon, H. Y.; Han, H. S.; Kim, S.-H.; Son, S.; Jo, D.-G.; Ahn,  
35     C.-H.; Suh, Y. D.; Kim, K.; Chan Kwon, I.; Lee, D. S.; Park, J. H. Hypoxia-Responsive  
36     Polymeric Nanoparticles for Tumor-Targeted Drug Delivery. *Biomaterials* **2014**, *35* (5),  
37     1735–1743. <https://doi.org/10.1016/j.biomaterials.2013.11.022>.  
38  
39  
40  
41  
42  
43  
44  
45  
46  
47  
48  
49  
50  
51  
52  
53  
54  
55  
56  
57  
58  
59  
60

1  
2  
3 (16) Kozlovska, V.; Liu, F.; Xue, B.; Ahmad, F.; Alford, A.; Saeed, M.; Kharlampieva, E.  
4 Polyphenolic Polymersomes of Temperature-Sensitive Poly(N-Vinylcaprolactam)-Block-  
5 Poly(N-Vinylpyrrolidone) for Anticancer Therapy. *Biomacromolecules* **2017**, *18* (8), 2552–  
6 2563. <https://doi.org/10.1021/acs.biomac.7b00687>.

7 (17) Confeld, M. I.; Mamnoon, B.; Feng, L.; Jensen-Smith, H.; Ray, P.; Froberg, J.; Kim, J.;  
8 Hollingsworth, M. A.; Quadir, M.; Choi, Y.; Mallik, S. Targeting the Tumor Core: Hypoxia-  
9 Responsive Nanoparticles for the Delivery of Chemotherapy to Pancreatic Tumors. *Mol.*  
10 *Pharmaceutics* **2020**, *17* (8), 2849–2863.  
11 <https://doi.org/10.1021/acs.molpharmaceut.0c00247>.

12 (18) Kulkarni, P.; Haldar, M. K.; You, S.; Choi, Y.; Mallik, S. Hypoxia-Responsive Polymersomes  
13 for Drug Delivery to Hypoxic Pancreatic Cancer Cells. *Biomacromolecules* **2016**, *17* (8),  
14 2507–2513. <https://doi.org/10.1021/acs.biomac.6b00350>.

15 (19) Golombek, S. K.; May, J.-N.; Theek, B.; Appold, L.; Drude, N.; Kiessling, F.; Lammers, T.  
16 Tumor Targeting via EPR: Strategies to Enhance Patient Responses. *Adv Drug Deliv Rev*  
17 **2018**, *130*, 17–38. <https://doi.org/10.1016/j.addr.2018.07.007>.

18 (20) Kulkarni, P.; Haldar, M. K.; Katti, P.; Dawes, C.; You, S.; Choi, Y.; Mallik, S. Hypoxia-  
19 Responsive, Tumor Penetrating Lipid Nanoparticles for Delivery of Chemotherapeutics to  
20 Pancreatic Cancer Cell Spheroids. *Bioconjugate Chem.* **2016**, *27* (8), 1830–1838.  
21 <https://doi.org/10.1021/acs.bioconjchem.6b00241>.

22 (21) Niu, S.; Bremner, D. H.; Wu, J.; Wu, J.; Wang, H.; Li, H.; Qian, Q.; Zheng, H.; Zhu, L. L-  
23 Peptide Functionalized Dual-Responsive Nanoparticles for Controlled Paclitaxel Release  
24 and Enhanced Apoptosis in Breast Cancer Cells. *Drug Delivery* **2018**, *25* (1), 1275–1288.  
25 <https://doi.org/10.1080/10717544.2018.1477863>.

26 (22) Miller-Kleinhenz, J. M.; Bozeman, E. N.; Yang, L. Targeted Nanoparticles for Image-Guided  
27 Treatment of Triple Negative Breast Cancer: Clinical Significance and Technological  
28

1  
2  
3 Advances. *Wiley Interdiscip Rev Nanomed Nanobiotechnol* **2015**, *7* (6), 797–816.  
4  
5 <https://doi.org/10.1002/wnan.1343>.  
6  
7 (23) Karandish, F.; Mamnoon, B.; Feng, L.; Haldar, M. K.; Xia, L.; Gange, K. N.; You, S.; Choi,  
8 Y.; Sarkar, K.; Mallik, S. Nucleus-Targeted, Echogenic Polymersomes for Delivering a  
9 Cancer Stemness Inhibitor to Pancreatic Cancer Cells. *Biomacromolecules* **2018**, *19* (10),  
10 4122–4132. <https://doi.org/10.1021/acs.biomac.8b01133>.  
11  
12 (24) Guan, L.; Rizzello, L.; Battaglia, G. Polymersomes and Their Applications in Cancer  
13 Delivery and Therapy. *Nanomedicine* **2015**, *10* (17), 2757–2780.  
14  
15 <https://doi.org/10.2217/nnm.15.110>.  
16  
17 (25) Martin, C.; Aibani, N.; Callan, J. F.; Callan, B. Recent Advances in Amphiphilic Polymers  
18 for Simultaneous Delivery of Hydrophobic and Hydrophilic Drugs. *Therapeutic Delivery*  
19 **2015**, *7* (1), 15–31. <https://doi.org/10.4155/tde.15.84>.  
20  
21 (26) Teesalu, T.; Sugahara, K. N.; Ruoslahti, E. Tumor-Penetrating Peptides. *Front Oncol* **2013**,  
22 3. <https://doi.org/10.3389/fonc.2013.00216>.  
23  
24 (27) Kulkarni, P.; Haldar, M. K.; Karandish, F.; Confeld, M.; Hossain, R.; Borowicz, P.; Gange,  
25 K.; Xia, L.; Sarkar, K.; Mallik, S. Tissue-Penetrating, Hypoxia-Responsive Echogenic  
26 Polymersomes For Drug Delivery To Solid Tumors. *Chemistry – A European Journal* **2018**,  
27 24 (48), 12490–12494. <https://doi.org/10.1002/chem.201802229>.  
28  
29 (28) Sugahara, K. N.; Teesalu, T.; Karmali, P. P.; Kotamraju, V. R.; Agemy, L.; Girard, O. M.;  
30 Hanahan, D.; Mattrey, R. F.; Ruoslahti, E. Tissue-Penetrating Delivery of Compounds and  
31 Nanoparticles into Tumors. *Cancer Cell* **2009**, *16* (6), 510–520.  
32  
33 <https://doi.org/10.1016/j.ccr.2009.10.013>.  
34  
35 (29) Krausz, A. E.; Adler, B. L.; Makdisi, J.; Schairer, D.; Rosen, J.; Landriscina, A.; Navati, M.;  
36 Alfieri, A.; Friedman, J. M.; Nosanchuk, J. D.; Rodriguez-Gabin, A.; Ye, K. Q.; McDaid, H.  
37 M.; Friedman, A. J. Nanoparticle-Encapsulated Doxorubicin Demonstrates Superior Tumor  
38  
39  
40  
41  
42  
43  
44  
45  
46  
47  
48  
49  
50  
51  
52  
53  
54  
55  
56  
57  
58  
59  
60

1  
2  
3 Cell Kill in Triple Negative Breast Cancer Subtypes Intrinsically Resistant to Doxorubicin.  
4  
5 *Precis Nanomed* **2018**, 1 (3), 173–182. [https://doi.org/10.33218/prnano1\(3\).181029.1](https://doi.org/10.33218/prnano1(3).181029.1).

6  
7 (30) Gref, R.; Minamitake, Y.; Peracchia, M. T.; Trubetskoy, V.; Torchilin, V.; Langer, R.  
8  
9 Biodegradable Long-Circulating Polymeric Nanospheres. *Science* **1994**, 263 (5153), 1600–  
10  
11 1603. <https://doi.org/10.1126/science.8128245>.

12  
13 (31) Anajafi, T.; Yu, J.; Sedigh, A.; Haldar, M. K.; Muhonen, W. W.; Oberlander, S.; Wasness,  
14  
15 H.; Froberg, J.; Molla, M. S.; Katti, K. S.; Choi, Y.; Shabb, J. B.; Srivastava, D. K.; Mallik,  
16  
17 S. Nuclear Localizing Peptide-Conjugated, Redox-Sensitive Polymersomes for Delivering  
18  
19 Curcumin and Doxorubicin to Pancreatic Cancer Microtumors. *Mol. Pharmaceutics* **2017**,  
20  
21 14 (6), 1916–1928. <https://doi.org/10.1021/acs.molpharmaceut.7b00014>.

22  
23 (32) Du, Y.; Chen, W.; Zheng, M.; Meng, F.; Zhong, Z. PH-Sensitive Degradable Chimaeric  
24  
25 Polymersomes for the Intracellular Release of Doxorubicin Hydrochloride. *Biomaterials*  
26  
27 **2012**, 33 (29), 7291–7299. <https://doi.org/10.1016/j.biomaterials.2012.06.034>.

28  
29 (33) Krishnamachary, B.; Penet, M.-F.; Nimmagadda, S.; Mironchik, Y.; Raman, V.;  
30  
31 Solaiyappan, M.; Semenza, G. L.; Pomper, M. G.; Bhujwalla, Z. M. Hypoxia Regulates  
32  
33 CD44 and Its Variant Isoforms through HIF-1 $\alpha$  in Triple Negative Breast Cancer. *PLOS*  
34  
35 **ONE** **2012**, 7 (8), e44078. <https://doi.org/10.1371/journal.pone.0044078>.

36  
37 (34) Liu, X.; Jiang, J.; Ji, Y.; Lu, J.; Chan, R.; Meng, H. Targeted Drug Delivery Using IRGD  
38  
39 Peptide for Solid Cancer Treatment. *Mol. Syst. Des. Eng.* **2017**, 2 (4), 370–379.  
40  
41 <https://doi.org/10.1039/C7ME00050B>.

42  
43 (35) Patel, A.; Sant, S. Hypoxic Tumor Microenvironment: Opportunities to Develop Targeted  
44  
45 Therapies. *Biotechnology Advances* **2016**, 34 (5), 803–812.  
46  
47 <https://doi.org/10.1016/j.biotechadv.2016.04.005>.

48  
49 (36) Confeld, M. I.; Mamnoon, B.; Feng, L.; Jensen-Smith, H.; Ray, P.; Froberg, J.; Kim, J.;  
50  
51 Hollingsworth, M. A.; Quadir, M.; Choi, Y.; Mallik, S. Targeting the Tumor Core: Hypoxia-  
52  
53  
54  
55  
56  
57  
58  
59  
60

1  
2  
3     Responsive Nanoparticles for Delivery of Chemotherapy to Pancreatic Tumors. *Mol.*  
4     *Pharmaceutics* **2020**. <https://doi.org/10.1021/acs.molpharmaceut.0c00247>.

5  
6     (37) Mamnoon, B.; Feng, L.; Froberg, J.; Choi, Y.; Sathish, V.; Mallik, S. Hypoxia-Responsive,  
7     Polymeric Nanocarriers for Targeted Drug Delivery to Estrogen Receptor-Positive Breast  
8     Cancer Cell Spheroids. *Mol. Pharmaceutics* **2020**, *17* (11), 4312–4322.  
9  
10     <https://doi.org/10.1021/acs.molpharmaceut.0c00754>.

11  
12     (38) Brownlee, W. J.; Seib, F. P. Impact of the Hypoxic Phenotype on the Uptake and Efflux of  
13     Nanoparticles by Human Breast Cancer Cells. *Scientific Reports* **2018**, *8* (1), 12318.  
14  
15     <https://doi.org/10.1038/s41598-018-30517-3>.

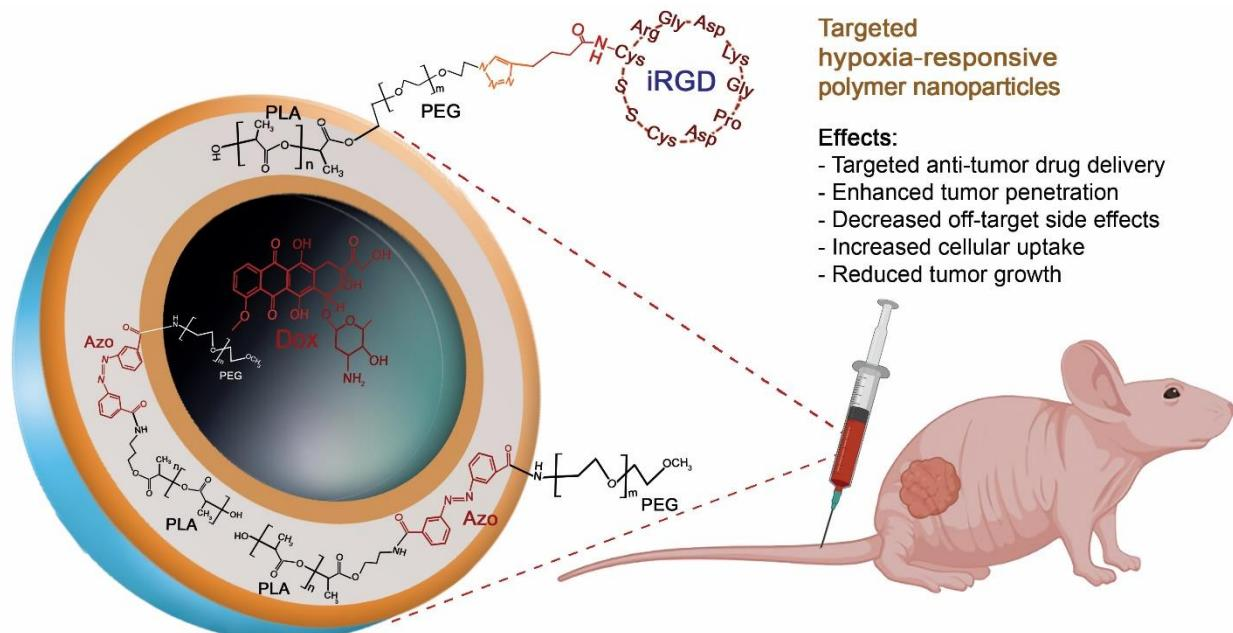
16  
17     (39) Cano-Cortes, M. V.; Navarro-Marchal, S. A.; Ruiz-Blas, M. P.; Diaz-Mochon, J. J.; Marchal,  
18     J. A.; Sanchez-Martin, R. M. A Versatile Theranostic Nanodevice Based on an Orthogonal  
19     Bioconjugation Strategy for Efficient Targeted Treatment and Monitoring of Triple Negative  
20     Breast Cancer. *Nanomedicine: Nanotechnology, Biology and Medicine* **2020**, *24*, 102120.  
21  
22     <https://doi.org/10.1016/j.nano.2019.102120>.

23  
24     (40) Dalmark, M. The Physicochemical Properties and Transmembraneous Transport of  
25     Doxorubicin. In *Anthracycline Antibiotics in Cancer Therapy: Proceedings of the*  
26     *International Symposium on Anthracycline Antibiotics in Cancer Therapy*, New York, New  
27     York, 16–18 September 1981; Muggia, F. M., Young, C. W., Carter, S. K., Eds.;  
28     Developments in Oncology; Springer Netherlands: Dordrecht, 1982; pp 165–172.  
29  
30     [https://doi.org/10.1007/978-94-009-7630-6\\_15](https://doi.org/10.1007/978-94-009-7630-6_15).

31  
32     (41) Zhang, P.; Yang, H.; Shen, W.; Liu, W.; Chen, L.; Xiao, C. Hypoxia-Responsive Polypeptide  
33     Nanoparticles Loaded with Doxorubicin for Breast Cancer Therapy. *ACS Biomater. Sci.*  
34     *Eng.* **2020**, *6* (4), 2167–2174. <https://doi.org/10.1021/acsbiomaterials.0c00125>.

35  
36  
37  
38  
39  
40  
41  
42  
43  
44  
45  
46  
47  
48  
49  
50  
51  
52  
53  
54  
55  
56  
57  
58  
59  
60

## Graphical Abstract



1  
2  
3  
4  
5  
6  
7  
8  
9  
10  
11  
12  
13  
14  
15  
16  
17  
18  
19  
20  
21  
22  
23  
24  
25  
26  
27  
28  
29  
30  
31  
32  
33  
34  
35  
36  
37  
38  
39  
40  
41  
42  
43  
44  
45  
46  
47  
48  
49  
50  
51  
52  
53  
54  
55  
56  
57  
58  
59  
60  

## Graphical Abstract:

Targeted hypoxia-responsive polymer nanoparticles

Effects:

- Targeted anti-tumor drug delivery
- Enhanced tumor penetration
- Decreased off-target side effects
- Increased cellular uptake
- Reduced tumor growth

ACS Paragon Plus Environment